Arabian Journal for Science and Engineering (2018) 43:4635–4647
https://doi.org/10.1007/s13369-017-3002-4

RESEARCH ARTICLE - MECHANICAL ENGINEERING

Measured Cutting Forces in the Turning of Prismatic Parts at Different Spindle Speeds and Side Cutting Edge Angles

Erkan Öztürk[1] · **Kemal Yıldızlı**[1]

Received: 14 July 2017 / Accepted: 23 November 2017 / Published online: 12 December 2017

Abstract
This study attempted to measure three cutting force components simultaneously for prismatic parts and determine the force-time characteristics until face turning was finished. A calibrated dynamometer was used in the turning experiments. The experiments for the aluminum alloy and brass workpieces were performed at different side cutting edge angles (SCEAs) for three different spindle speeds. The turning finishing processes of the prismatic parts were also monitored successfully. The cutting speed had a remarkable effect on the quality of data acquisition, but the SCEA did not. The scatter width of all forces increased with decreasing cutting speed, but the SCEA was not effective. Three forces generally exhibited familiar characteristic with increment in the SCEA for aluminum and brass workpieces. Furthermore, the cutting force amplitudes were perceived to be higher in cylindrical machining regions than impact machining regions. The F_c and F_r indicated similar self-trends for both metals during total machining processes.

Keywords Prismatic parts · Turning · Machining · Cutting forces

1 Introduction

Cutting tools are exposed to cutting forces (F_c, F_f and F_r)[1] in turning applications. In conjunction with the geometry of the workpiece and cutting tool, cutting forces are also affected by the cutting parameters, e.g., rake angle, side cutting edge angle (SCEA), depth of the cut and tool feed. Thus, machining parameters may cause remarkable changes in the cutting forces. Previous published studies focused on different fields of machining tools. For examples, cutting force dynamometer designs [1], either the combined or individual effect of the cutting parameters [2–9], the enhancement of surface roughness and machinability [9–17], better diametric accuracy [18,19], and tool wear and fracture [20–23] were investigated by computer-aided modeling or experiments.

Direct force measurements for turning operations were generally realized by three main sensor types as load cells, piezo-electric dynamometers (Kistler table dynamometers) and strain gage-based dynamometers. Load cells are generally used for sensing high, static or slowly changing cutting force data via little deflection [24]. Different studies were performed with using these type dynamometers. For example; a study searched the rake angle effects on three cutting forces with using a self-designed force dynamometer comprised of two load cells [5]. Kistler table dynamometers uses piezo-electric effects. Forces act on the piezo-electric materials, and they transfer to voltages. This voltage changes provide measurement. Piezo-electric dynamometers can measure the cutting forces in three axis (X, Y and Z). Also, these dynamometers can perceive the small changes. They are clamped between the workpiece and the pallet. They are also center of attention for researchers. For example, Kong et al. improved a multi-task dynamometer that can allow flexible/automated tool change for different working conditions at industry. The researchers designed the dynamometer with using Kistler table dynamometer [25]. In the different study, some experiments were performed to predict the cutting forces and certain dynamic features on the tool tip. The authors used a single point diamond tool (SPDT). They used piezo-electric dynamometer for the experiments. They

[1] F_c: The main cutting force (N); F_f: Feed force (N); F_r: Radial force (N).

✉ Kemal Yıldızlı
kyildizli@omu.edu.tr

Erkan Öztürk
erkan.ozturk@omu.edu.tr

[1] Department of Mechanical Engineering, Engineering Faculty, Ondokuz Mayıs University, 55200 Atakum, Samsun, Turkey

investigated the effects of the cutting parameters [26]. Some researchers directed to use strain gage-based dynamometers to measure the cutting forces because these dynamometers offer reasonably high frequency response and long-term stability as with piezo-electric dynamometers [27]. Also, these dynamometers are modified directly from cutting tool. Thus, they are cheap and simple setup for manufacturing. Yaldız et al. performed two different study to measure the cutting forces with strain gage-based dynamometer. In their first study, a strain gage-based dynamometer, which can measure static and dynamic forces, were designed and manufactured. They used octagonal rings in their design. They evaluated the static and dynamic behaviors of the dynamometer subjected to linearity test, cross-sensitivity test, eccentricity test and performance test. They cited that the design was reliable [1]. In their second study, they used the same dynamometer. They calculated the orientation of the rings and position of the strain gages to improve the cross-sensitivity [28]. Panzera et al. performed another study to measure the cutting forces with using strain gage-based dynamometer. They integrated a cylindrical bar to their design, which had sensitivity to torsion and bending. They compared the results collected from designed dynamometer with data collected from piezo-electric dynamometer [29]. Zhao et al. investigated the cross-sensitivity of the three cutting force components. They improved the previous study published in 2006 with using the same design concept [30]. They cited that the cross-sensitivity was minimized. In the different study, a low cost compact dynamometer using with strain gages were designed and developed for high-speed turning. They used an innovative tool shank at their design and determine the orientation of the strain gages. They cited that the cross-sensitivity was very small and negligible. Also, they tested their design experimentally [31]. Öztürk and Yıldızlı attempted to manufacture a new static calibration methodology for strain gaged based dynamometer. The authors used the known design criteria for strain gage-based dynamometer to manufacture. However, they investigated the cross-sensitivity of the forces and proposed a mathematical and statistical approach to eliminate the cross-sensitivity. They cited that this approach could enable to eliminate the cross-sensitivities [32].

Because of the rigidity and brittleness of the tool inserts, it seems difficult to increase the cutting tool life and performance against impacts. For systematic analyses, impact magnitudes, frequency and time spans should be determined for a cutting tool design on turning. Although the turning of prismatic parts does not take in account recent studies, it is actively used in metal cutting applications. If the tool insert is broken, controlling the cutting parameters is less important. The fractures can result from overloading, impacts and chip compression, while the insert is in contact with the workpiece surface. Special insert coatings that quantify the surface roughness and minimize the built-up edge were developed to increase the tool performance in previous studies [12,22,33,34]. Additionally, the geometrical modeling of the tool-workpiece interaction was investigated [13,35,36]. Another different study searched the performance of micro grooved polycrystalline diamond tool for Ti6Al4V titanium alloy in dry machining [37]. However, researchers were not interested in paradoxes in any impact regimes. Although the cutting forces acting on inserts can be measured, the impact strengths are detected by fracture mechanics, guide information and field works at an industrial scale. It is known that the cutting forces and tool wear has been investigated to improve the design and proper application of the cutting tool. Researchers turned to intermittent turning to investigate the tool wear and tool life [38,39]. They used slotted or ribbed workpieces which create high impact loads on the cutting tool and they emphasized that impact loads effect on tool life, surface quality and dimension accuracy negatively. The impact loads can be monitored and searched with not only intermittent turning but also turning prismatic parts. Therefore, in-situ force measurement is required to investigate variable cutting forces at periodical impacts, and this is possible by machining prismatic workpieces. The solid sectioned prismatic parts, such as profiles and bars, are locally transformed into cylindrical geometry by machining in turning lathes. The serial manufacturing of pressure gauge sockets made of brass or aluminum alloy is a good example of a prismatic machining process. Also, large-scale prismatic parts can be machined in industry applications (Fig. 1). When the prismatic metals are machined, an investigation of the cutting forces can reveal different approaches on the fracture of the inserts.

In this study, square sectioned prismatic aluminum alloy and brass workpieces were machined on a turning lathe instead of the routine circular sectioned workpiece. During the experiments, the cutting forces were measured simultaneously. For this purpose, a strain gage integrated force dynamometer was designed and produced from a cutting tool. Finally, a series of machining experiments were performed to reveal variable regimes of the cutting force components acting on the cutting tool in the machining of the prismatic parts.

2 Materials and Methods

The cutting force components acting on a cutting tool are commonly measured with dynamometers or transducers. These devices work according to the measurement of the surface strain on elastic elements. However, all elements do not have enough flexibility. Thus, strain gage integrated force dynamometers should be used [41].

In this research, a tool dynamometer was designed and manufactured to measure the cutting force components for turning. Afterward, the dynamometer was connected to a data logger. The data logger and PC were also inter-

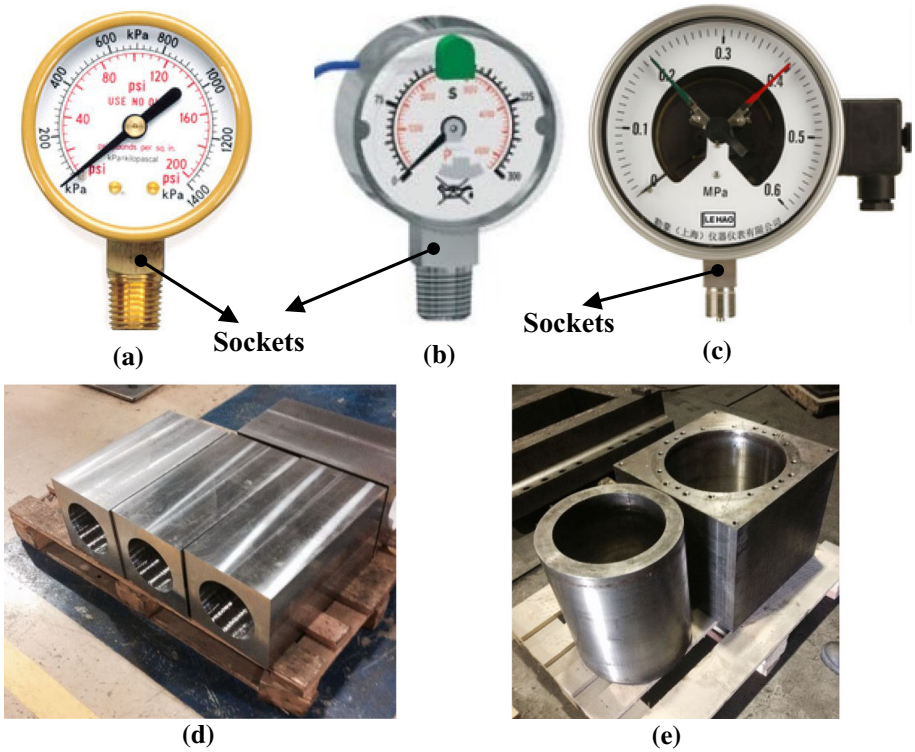

Fig. 1 Pressure gauge (**a**), contact gauges (**b**), electrical contact gauges (**c**) [40] and large-scaled prismatic parts (**d**), (**e**) (by courtesy of Durmazlar Makina Inc.)

connected. After the dynamometer was calibrated by a loading/unloading procedure [42], a series of experiments were performed at the machining of the metal prismatic workpieces. The dynamometer design, calibration and manufacturing process of the dynamometer were reported in elsewhere [32].

2.1 Workpieces, Insert and Holding Device

Square sectioned aluminum alloy and brass workpieces[2] measuring $20 \times 20\,\text{mm}^2$ were used for the experiments in this study. One side of the workpieces was transformed to a cylindrical shape to hold the spindle, while the other side stayed prismatic. The chemical compositions of the workpieces are given in detail in Table 1. Boehlerit brand insert was selected to machine both of the materials. To hold the cutting tool on the tool post and keep the overwhelming distance constant, a tool holder was designed and manufactured (Fig. 2f).

2.2 Design and Construction of the Dynamometer

The dynamometer was formed by modifying a cutting tool with twelve strain gages (Kyowa brand N11MA212011 type). The strain gages were placed on the tool surface. The dynamometer had three channels for measuring F_c, F_f and F_r. Each channel could measure one force component, and the three channels could work simultaneously. Each channel was connected with a full Wheatstone bridge circuit (FWBC). The small sectioned cutting tool was selected. The tool, which is Boehlerit brand and SCLC-R type, has a $10 \times 10\,\text{mm}^2$ square section. Thus, the dynamometer could easily sense strain changes under any loading. The directions of the cutting forces, the FWBC and the positions of the strain gages on the tool surface for each force component are presented in Fig. 2a–e.

2.3 Measurement and Test Configuration

In this study, an HBM brand DQ430 type dynamic strain gage amplifier was used. This data logger has hardware and software to measure strain voltage signals and transfer data to a computer. It has four data transfer channels that can work simultaneously. Because the data logger can measure the three force components simultaneously, a comprehensive system was configured along with a universal turning lathe, a designed force dynamometer, a data logger and a personal computer. The configured measurement system is shown in Fig. 2f.

2.4 Calibration of the Dynamometer

The dynamometer must be calibrated after production. The voltage signals (mV/V) arising from the elastic deformation

[2] There are three reasons for selecting aluminum and brass, namely, easy machinability, not to break the insert, and being materials of pressure gage sockets.

Table 1 Chemical compositions of prismatic metal workpieces

Materials	Element (wt%)															
Aluminum (AA6061)	Si	Fe	Cu	Mn	Mg	Cr	Zn	Ni	Ti	V	Pb	Ga	Sb	Zr	Al	
	0.965	0.608	0.669	0.522	0.858	0.031	0.259	0.010	0.016	0.011	0.014	0.013	0.005	0.013	96.00	
Brass (MS58)	Si	Fe	Cu	Mn	Mg	Cr	Zn	Ni	Sn	P	Pb	Co	Sb			
	0.006	0.460	58.318	0.014	0.002	0.008	37.401	0.220	0.283	0.004	3.107	0.034	0.063			

of the cutting tool were converted to units of force (Newton) during the calibration process.

In this study, the calibration process of the cutting forces was performed at two stages using standard weights (each one is 10 N). In the first stage, two static calibration setups were designed and constructed to transfer certain weights to the dynamometer in the axial directions of each force component. These calibrators were made of steel to provide rigidity. The dynamometer was positioned parallel to the assembly floor and attached on a groove on the calibrator, and then, certain static loads were applied on the cutting tool insert. The output voltage signals were measured as the loads acted on the insert in increasing and decreasing sequences. The loads were selected in a range of 0–200 N and did not exceed the maximum loads in the experiments. In the second stage, the cross sensitivity (three-axial interaction) of the three force components was investigated separately. In the calibration process, each force component was calibrated by applying loads in the reference directions. All force components were measured and recorded. Afterward, the cross-sensitivities of the force components were compensated with curve fitting functions, which convert the output voltage signals to units of force. These generated functions are listed below. Moreover, all calibration measurements were repeated three times and verified to have statistically close values using SPSS [32,42].

$$F_c(x) = 1658.381732997173(x) - 0.4505506844001417 \quad (1)$$

$$F_f(x) = 1736.113182780943(x) + 0.6281882998717236 \quad (2)$$

$$F_r(x) = -43510078.69080053(x^3) + 1191267.477513403(x^2) + 5975.926328142997(x) - 3.146378074522424 \quad (3)$$

x: The output voltage signal

2.5 Experimental Procedure

A series of experiments were performed by machining prismatic metal workpieces in a universal turning lathe. In the experiments, the depth of the cut and feed were kept constant, and the SCEAs were changed in three different spindle revolutions per minutes (rpm). Four different SCEAs (0°, 5°, 10° and 15°) were chosen for the machining process at each revolution. Aluminum and brass prismatic workpieces $20 \times 20\ \text{mm}^2$ in size were used, and twelve experiments were conducted for each material in the turning lathe as a face turning application. The experimental schedule for the machining process is represented in Table 2.

During the experiments, data were collected and recorded every 0.02 s via the calibrated dynamometer. From the initial contact of the insert and workpiece corner, the cutting tool continued machining to the center point of the workpiece. The cutting forces acting on the cutting tool were measured. Then, their characteristics and magnitudes were represented

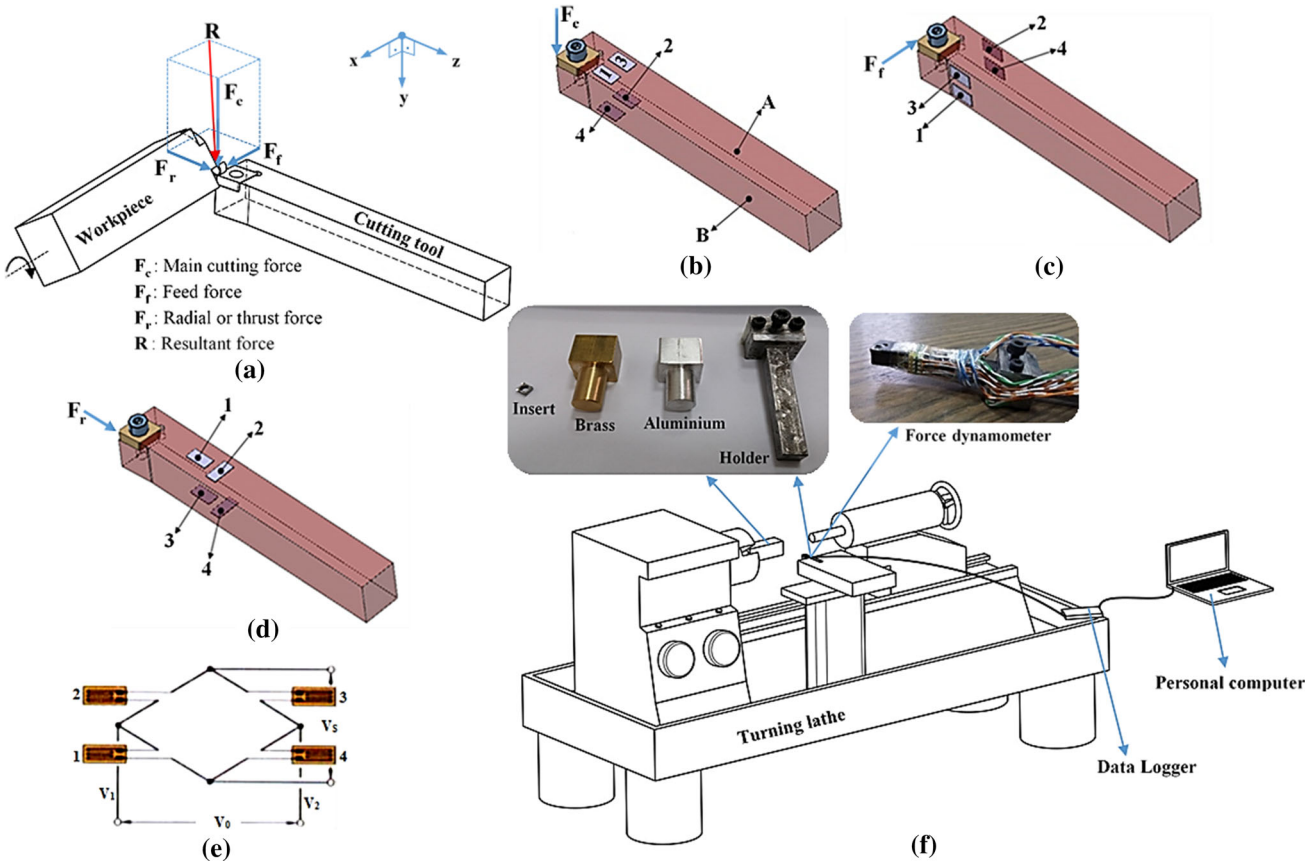

Fig. 2 Cutting force components (**a**), strain gage positions to measure the component of **b** F_c, **c** F_f and **d** F_r, the full Wheatstone bridge configuration (**e**) and the schematic representation of the cutting force measurement system (**f**)

Table 2 Machining parameters for aluminum (AA6061) and brass (MS58) workpieces

The machining geometry of face turning application for a prismatic part	Revolution (rev/min)	Maximum cutting speed (m/min)	Side cutting edge angle (°)	Depth of cut (mm)
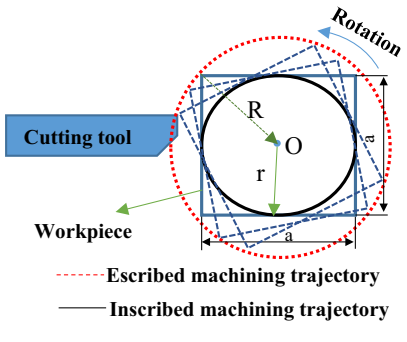	555 (fast)	49	0	0.05
			5	
			10	
			15	
	305 (medium)	27	0	0.05
			5	
			10	
			15	
	170 (slow)	15	0	0.05
			5	
			10	
			15	

Feed depth is 0.4 mm, and rake angle is 0° at all experiments

as force-time graphs for each experiment. All graphs were separated into three regions. The first region was called the impact region, which is the process of chip removal from the workpiece corner to a cylindrical shape. In the second region, the cylindrical machining process was performed. Lastly, turning was finished in the third region by pillar removal.

3 Results and Discussions

3.1 The Cutting Force Measurements for the Aluminum Workpiece

In the experiments, chip removal was performed at 555, 305 and 170 rpms, respectively, at 0°, 5°, 10° and 15° SCEAs (Figs. 3, 4, 5). If the plots are compared in Region 1 for 3 rpms, the cutting force components showed similar character for the four different angles. The F_c and F_f components increased. The reason for this result is the impacts when the workpiece corners hit the insert of the cutting tool. As the amount of chip removal from the corners rises, these forces must increase. For the cutting tool to move through the origin of the workpiece at a constant speed, it applied the same pressure on the workpiece contact area, and F_r did not change much. In the radial direction, the tool cannot be deflected easily, unlike the other force directions. However, the data overlapping the curves were revealed at 170 rpm (Fig. 5). F_c and F_f increased with much scatter, and F_r stayed nearly constant. The scattered band of the forces arose from the low rpm. Because of the low rpm, more signals could be taken during the metal cutting process. In Region 2, the prismatic machining finished, and cylindrical machining started for three rpms. The F_r and F_f components exhibited steady-state characteristics for all experiments from 0° to 15°, but F_r at 170 rpm (increased slightly). F_f was distributed as a line trend, whereas F_c followed a zigzag path. As the angle increased, the zigzag path was detected to be much more regular, and the measured cutting forces did not change significantly. In Region 3 for all rpms, machining operations end with the removal of the micro-sized pillar left at the center of the workpieces. When the micro-sized pillar breaks away from the workpiece center, the uniform chip removal as Region 2 cannot occur. After the cutting tool forces the micro-sized pillar to fracture, the tool travels without cutting. Therefore, the cutting forces presented unstable behaviors.

Three experiments were conducted for each SCEA. As the revolution decreased, the cutting forces showed small differences. Therefore, it could be deduced that they stayed mainly constant, which might arise from using the universal turning lathe. In addition, as the rpm decreased, the scatter width of the force distributions was wider in Region 1. Because of the rpm decrease, the data logger could catch and transfer more signals from the contact points during the machining. For that reason, more scattered distributions were observed.

It was seen that F_r was nearly unchanged, but negative, in the twelve experiments. This situation explains why the

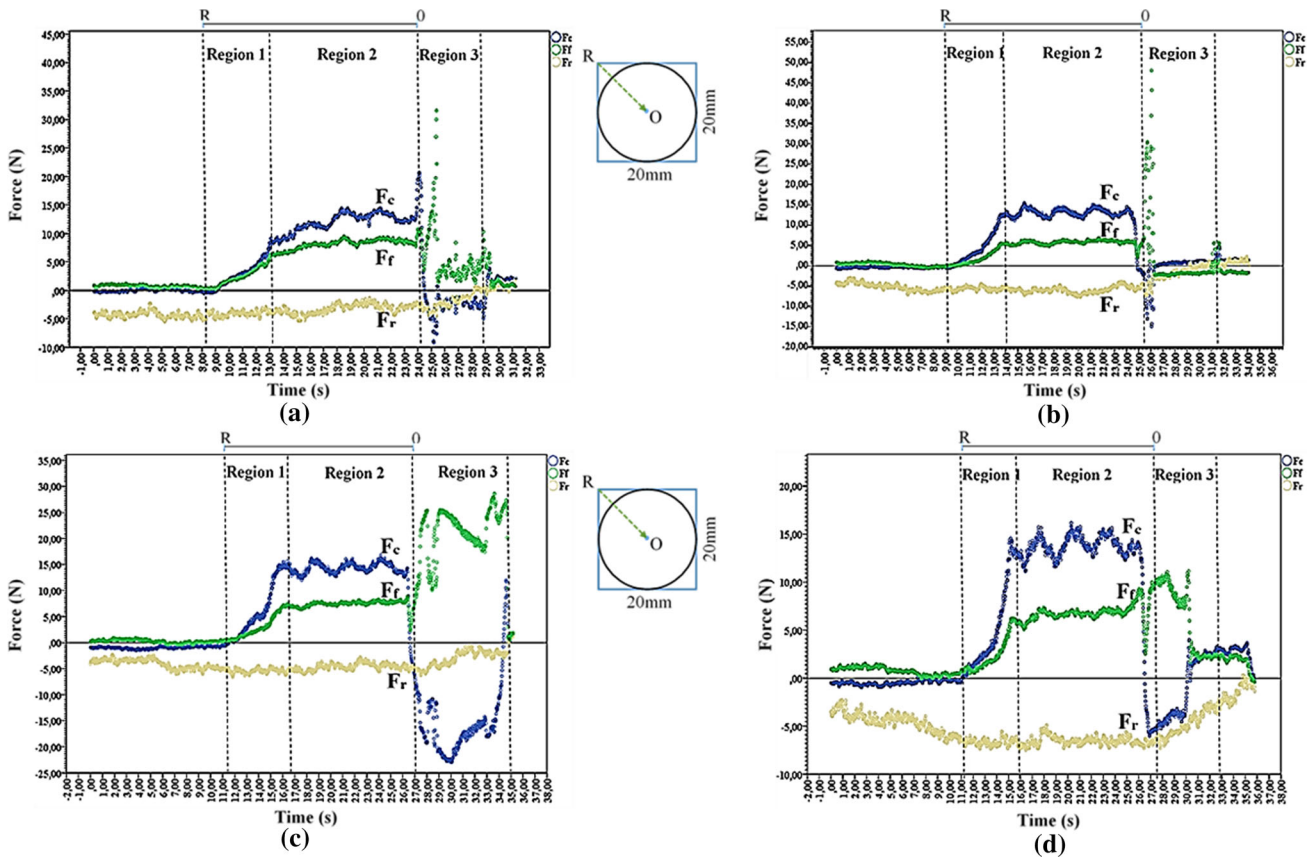

Fig. 3 The cutting forces acted on the cutting tool at **a** 0°, **b** 5°, **c** 10° and **d** 15° side cutting edge angles for 555 rpm machining operation

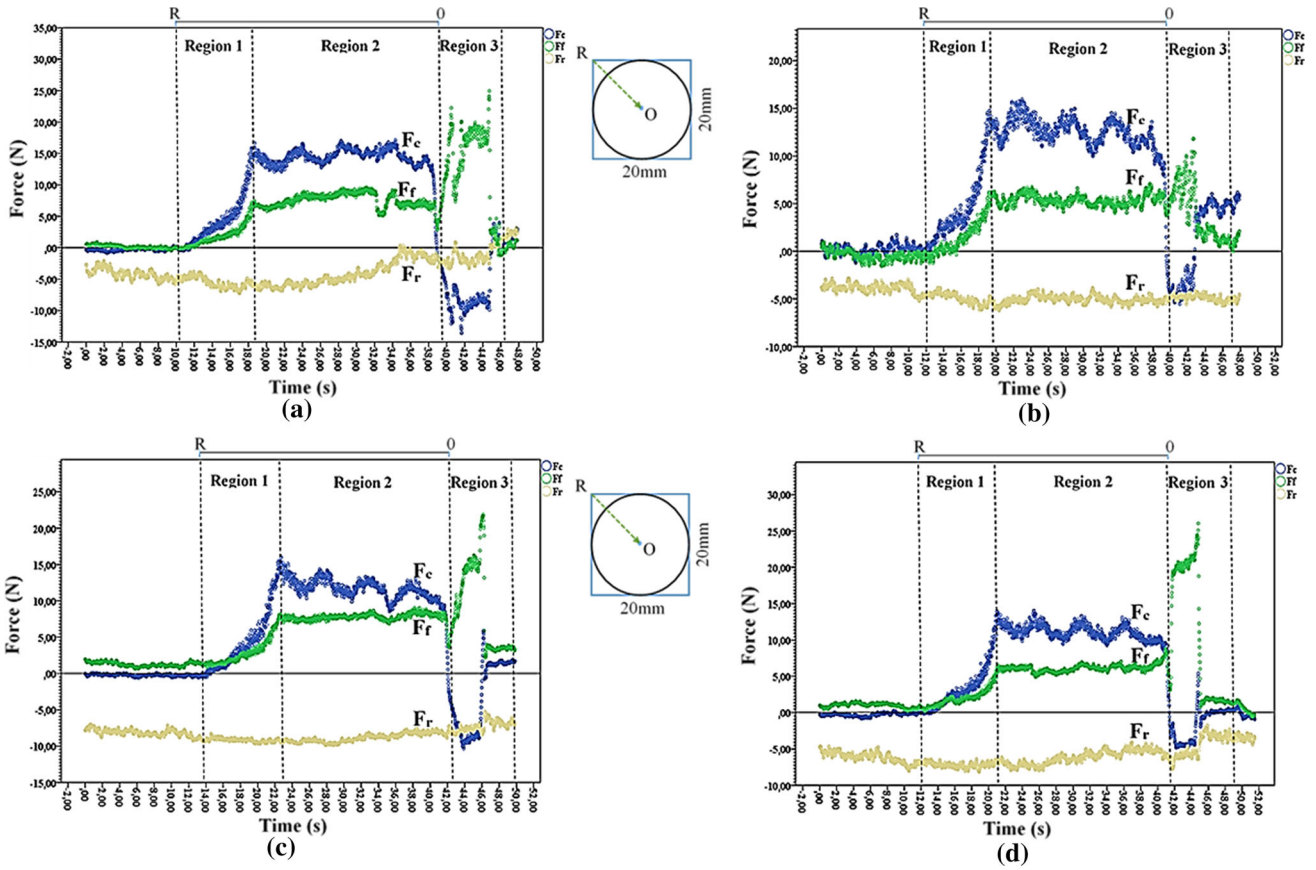

Fig. 4 The cutting forces acted on the cutting tool at **a** 0°, **b** 5°, **c** 10° and **d** 15° side cutting edge angles for 305 rpm machining operation

remarkable forces did not act on the cutting tool. In Region 1, F_r stayed constant and at its lowest value, but it increased slightly in Region 2. The change range of F_r during operation was found to be too small, and the F_r calibration function had a constant coefficient of − 3.15. Therefore, the F_r magnitudes in the experiments could not exceed the digit error of the F_r calibration equation.

Some researchers worked on behaviors of the cutting forces under the effects of cutting parameters such as cutting speed, feed rate, depth of cut, tool rake angle and approaching angle etc. for different cylindrical shaped materials. Two studies published in 2005 and 2006 cited that tool rake angle influences the cutting forces remarkably. Their most significant result was that F_c was decreased by increasing in positive rake angles [4,5]. Another different study investigated the effects of approaching angle (45°–90°) on the cutting forces. The authors cited that optimum approaching angle was obtained as 60°–70° and the greater approaching angles produced greater F_f, but less F_r [7]. In this study, the cutting forces were investigated under the effect of SCEAs in range of 0°-15°. It was observed that the SCEAs did not affect magnitudes of the cutting forces reasonably in region 2. This is shown in Fig. 6a–c. However, F_c followed a zigzag path and the zigzag path took more regular and symmetrical form in the increase of SCEAs. This zigzag path can be related to the chip removal motion on the cutting zone indicated in Fig. 6d. During chip removal motion, the forces acted on the tool tip could decrease with shortening in the length of the cutting zone until the chip breaking occurred. Increasing in SCEAs, the chip removal process repeated periodically in less time.

3.2 The Cutting Force Measurements for the Brass Workpiece

Four experiments were performed at each rpm (555, 305 and 170) (Figs. 7, 8, 9). In Region 1, the cutting forces showed similar characteristics for all SCEAs. F_c increased periodically for each rpm. The reason of this increment was the hits from the workpieces corners. Additionally, the removal chip areas increased during machining, so the impact forces increased, too. Because the tool movement through the workpiece origin was at a constant speed, F_r applied the same thrust on the cutting tool insert. Therefore, F_r stayed stable for all rpms. F_f showed a steady-state distribution during machining at all angles for all rpms. Nevertheless, F_c was

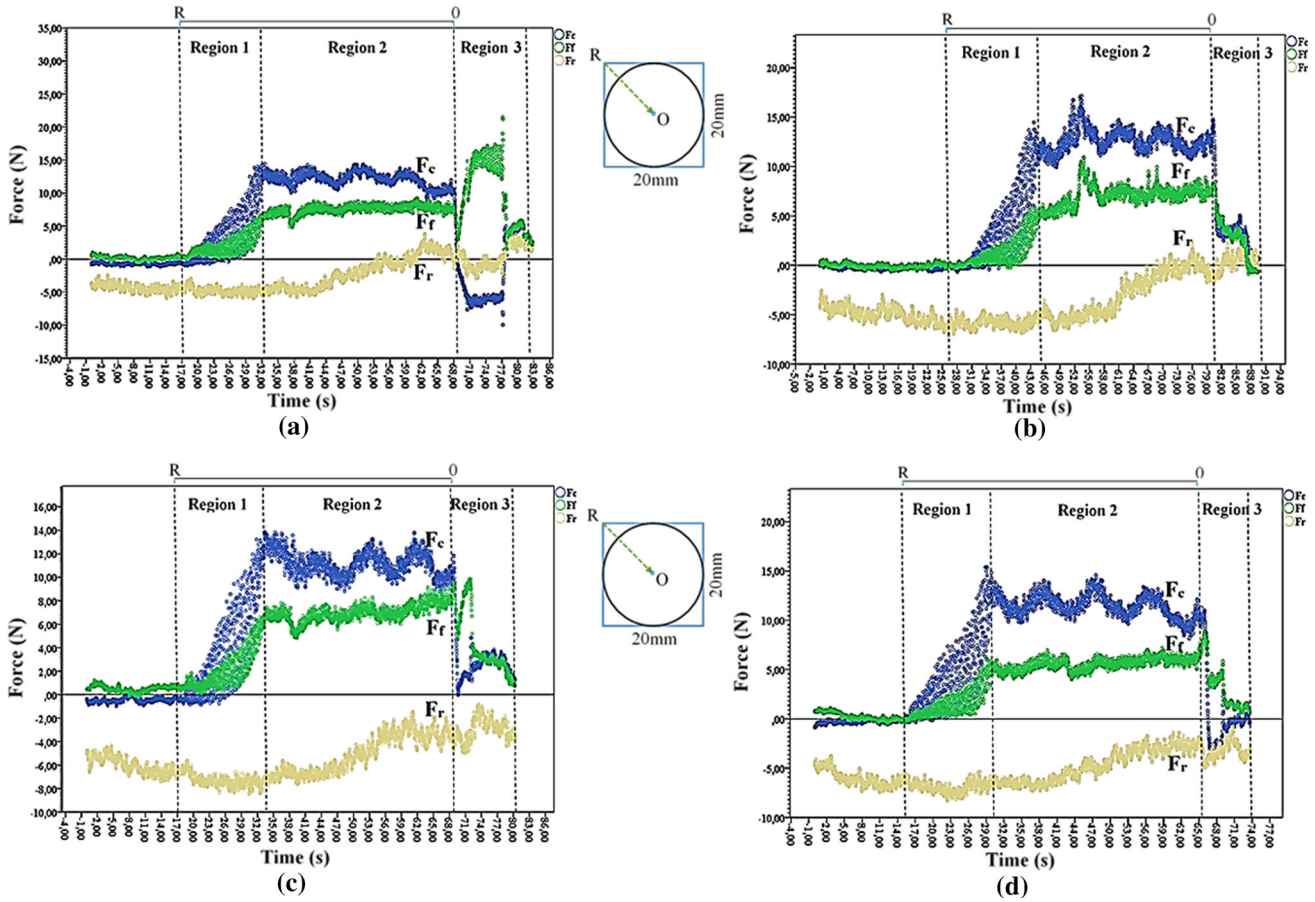

Fig. 5 The cutting forces acted on the cutting tool at **a** 0°, **b** 5°, **c** 10° and **d** 15° side cutting edge angles for 170 rpm machining operation

Fig. 6 The cutting forces acted on the cutting tool at **a** 555 rpm, **b** 305 rpm, **c** 170 rpm and face turning (**d**) for Region 2

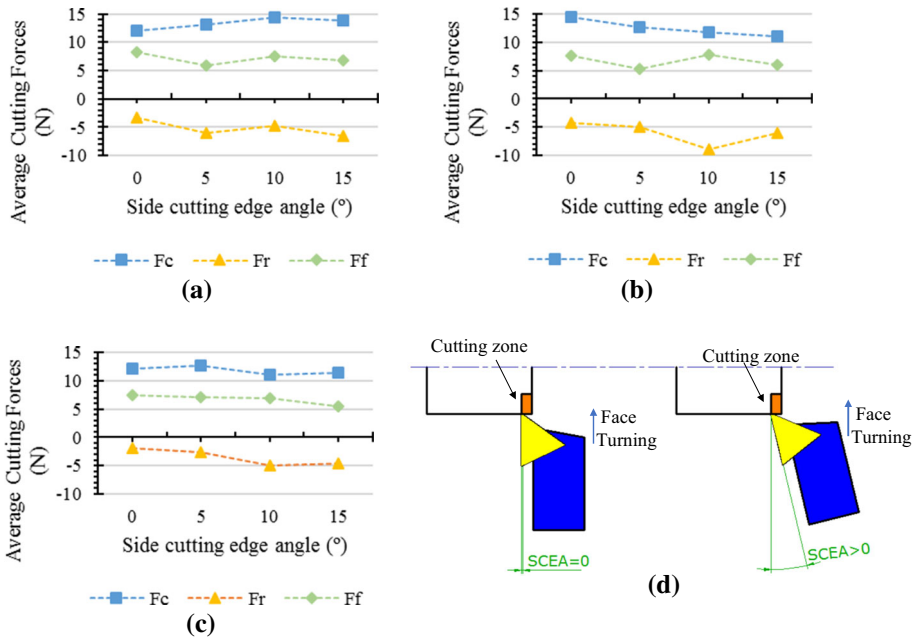

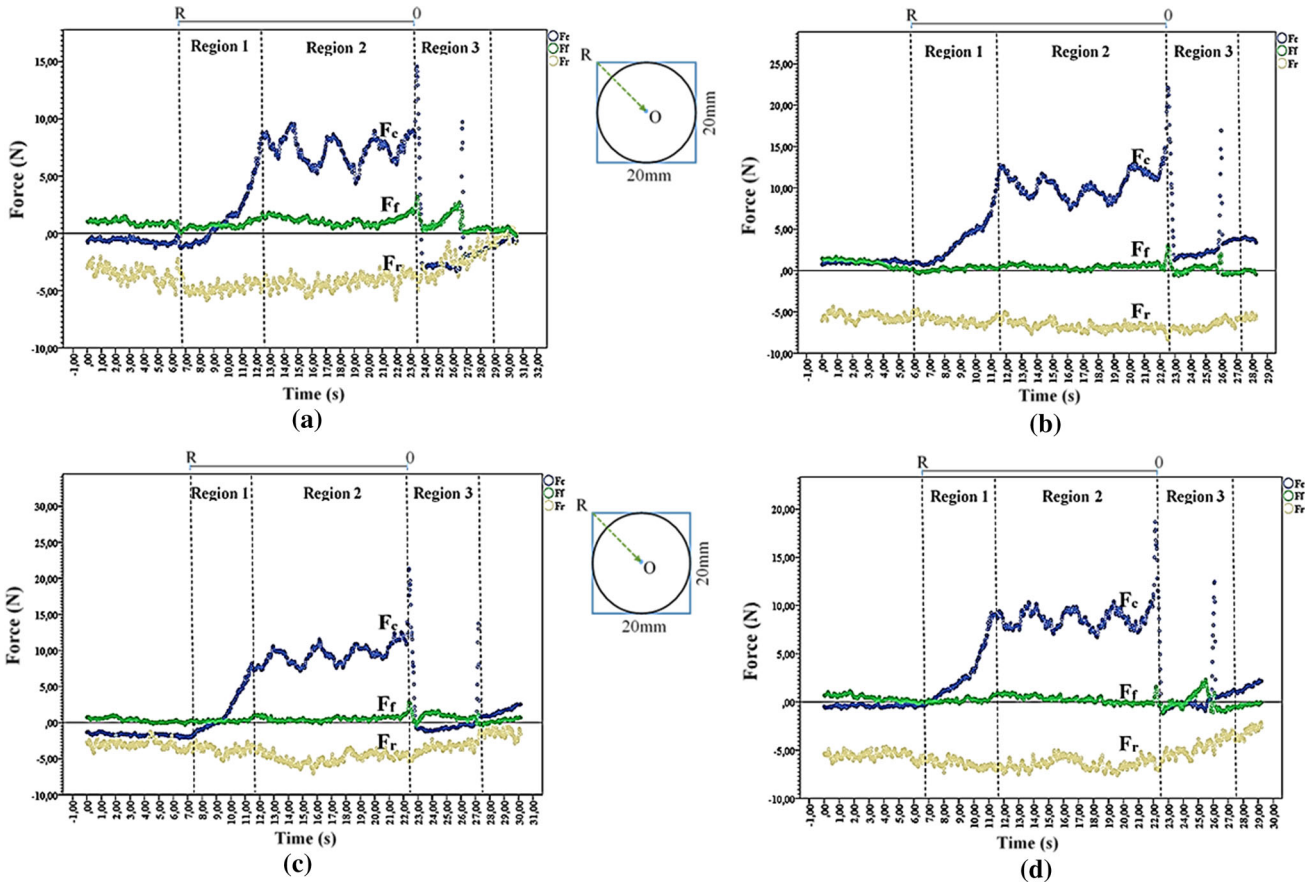

Fig. 7 The cutting forces acted on the cutting tool at **a** 0°, **b** 5°, **c** 10° and **d** 15° side cutting edge angles for 555 rpm machining operation

scattered in wide range and increased for 170 rpm. The scattered band resulted from the slow rpm because more data were obtained with the data logger in the machining operations. In Region 2, whereas F_c presented a periodically zigzag distribution based on the chip plowing and removing cycles, F_f and F_r were not affected significantly for all experiments. With an increase in the SCEA, F_f and F_r did not significantly change, but F_c showed a more regular zigzag-shaped distribution. Generally, the force amplitudes did not change. However, F_r increased slightly at the end of the Region 2 with decrease in rpm. In the last region, the turning operation was finished, and the forces had an irregular character as aluminum experiments.

In summary, the experiments were evaluated according to three sets of rpm values and four different SCEAs. As the rpm decreased, the cutting forces indicated slight differences. Therefore, it can be deduced that the forces did not change significantly as the rpm changed, which could result from the universal turning lathe. As the rpm decreased, the scatter width of the force distributions increased in Region 1. In the case of a slow rpm, more data were obtained and transferred to the computer. F_r was almost unchanged, but negative, in all experiments. This result was because of the small F_r acting on the insert exceeded the rigid error of the calibration function.

It was observed that the effect of SCEAs on magnitudes of the cutting forces was not considerably in region 2 as Aluminum experiments (Fig. 10). However, F_c followed a zigzag path too and the zigzag path became more regular 'V' shape as the increase of SCEAs. This zigzag path can be caused from the same reason mentioned before.

3.3 The Regime of the Cutting Forces Resulting from the Impacts

Measuring the impact forces is more difficult than measuring the forces in the cylindrical machining region. Because of this reason, Region 1 was more thoroughly analyzed.

The impact forces indicated similar distributions at Region 1. For that reason, one experiment was selected and interpreted for aluminum and brass. To understand the force regime easily in Region 1, the experiments having fewer data were selected. Therefore, Figs. 3a and 7a were zoomed in on and defined clearly (Fig. 11).

In the plots, F_c showed an irregular zigzag-shaped trend and increased sharply for two types of metals. This zigzag

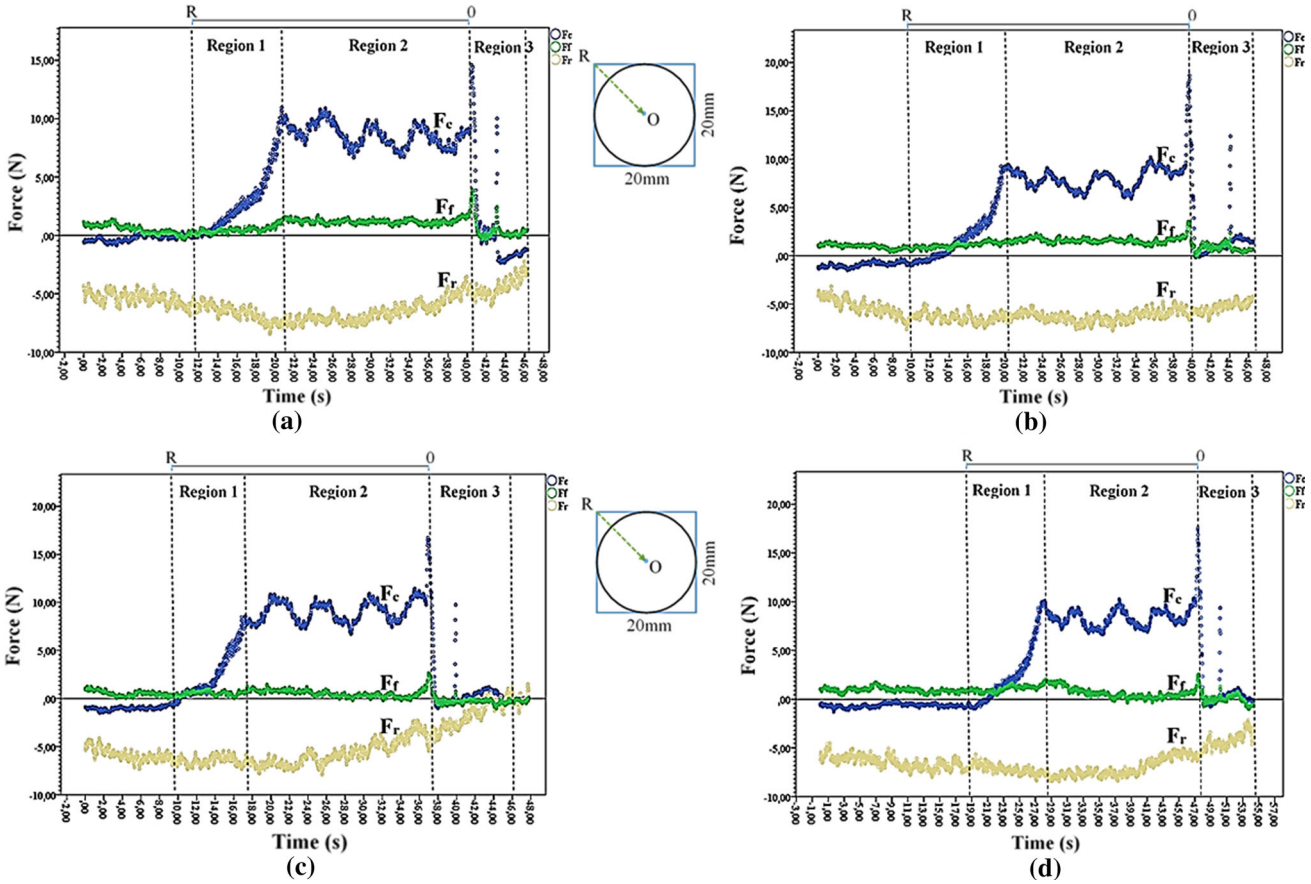

Fig. 8 The cutting forces acted on the cutting tool at **a** 0°, **b** 5°, **c** 10° and **d** 15° side cutting edge angles for 305 rpm machining operation

shape means that the forces acted on the tool insert during the corner movements of contacts in the machining process. In the contact moments, the force points followed a path that rose and fell. This decrease resulted from the small amount of contact time that was avoided while the cutting tool insert was passing from one corner to another. Whereas F_f increased in aluminum alloy, it had a stable machining regime for brass. As for F_r, it was stable and had a similar regime in the two metals.

4 Conclusions

Prismatic parts were machined with face turning. The SCEA was changed in the series of turning experiments, and F_c, F_f and F_r were measured simultaneously. Afterward, the force components were plotted as graphical outputs and discussed in the three regions. The results are outlined below.

- The fashion of the cylindrical machining process and the impact and turning finishing processes was clearly digitalized for both metals.
- In Region 1, F_c increased sharply for both materials. F_f increased for aluminum, but it stayed stable for brass. F_r stayed stable for both metals.
- In Region 2, F_c had a regular and periodic zigzag path as a 'v' shape, and F_f followed a stable straight line for both materials. F_r stayed stable at medium and fast rpm, but it increased slightly for slow rpm for both metals.
- In Region 3, it was understood that the turning operation finished, and the three force components showed unstable regimes for the aluminum and brass samples.
- As the SCEA changed, the force components showed familiar behavior for brass and aluminum alloy, but they scattered in different amplitudes. Additionally, a 15° increase did not change the magnitude much for all force components in the experiments.
- As the spindle speed increased, the scatter width of all force components decreased for both metals. There was more contact between the dynamometer and the workpiece so that the data logger perceived more signals. However, the spindle speed did not affect the force magnitudes significantly.

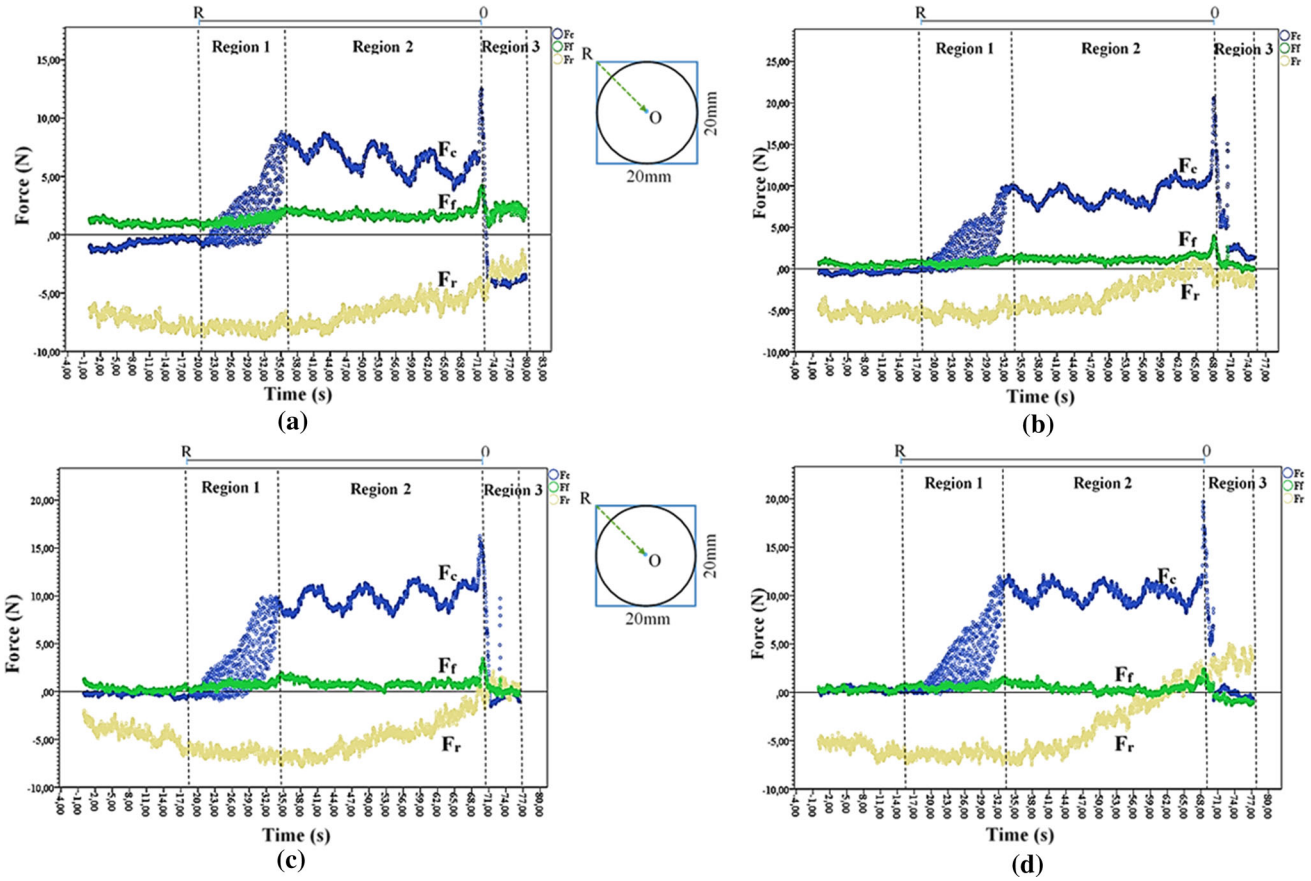

Fig. 9 The cutting forces acted on the cutting tool at **a** 0°, **b** 5°, **c** 10° and **d** 15° side cutting edge angles for 170 rpm machining operation

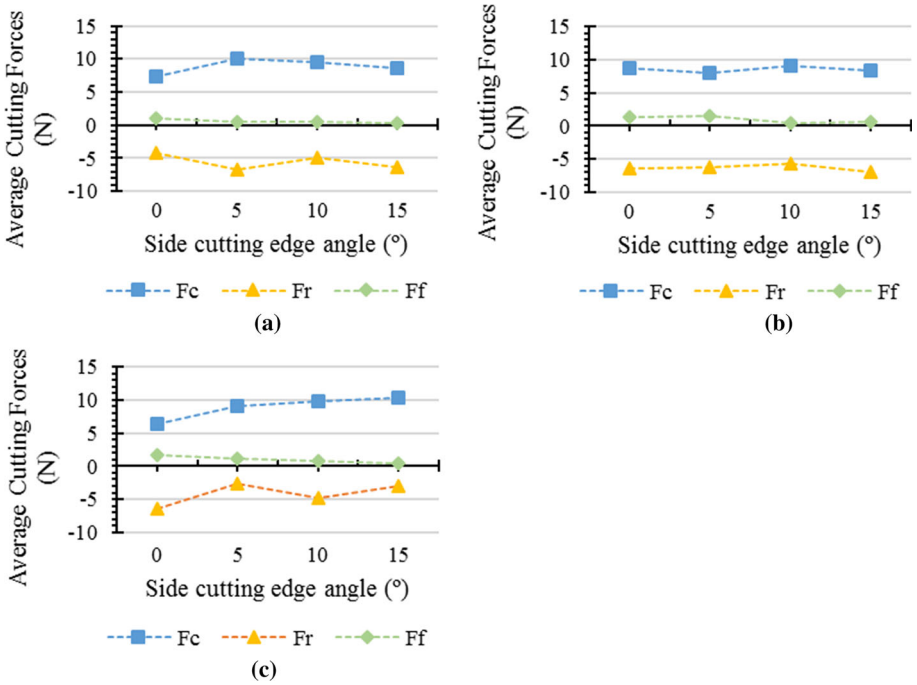

Fig. 10 The cutting forces acted on the cutting tool at **a** 555 rpm, **b** 305 rpm, **c** 170 rpm for Region 2

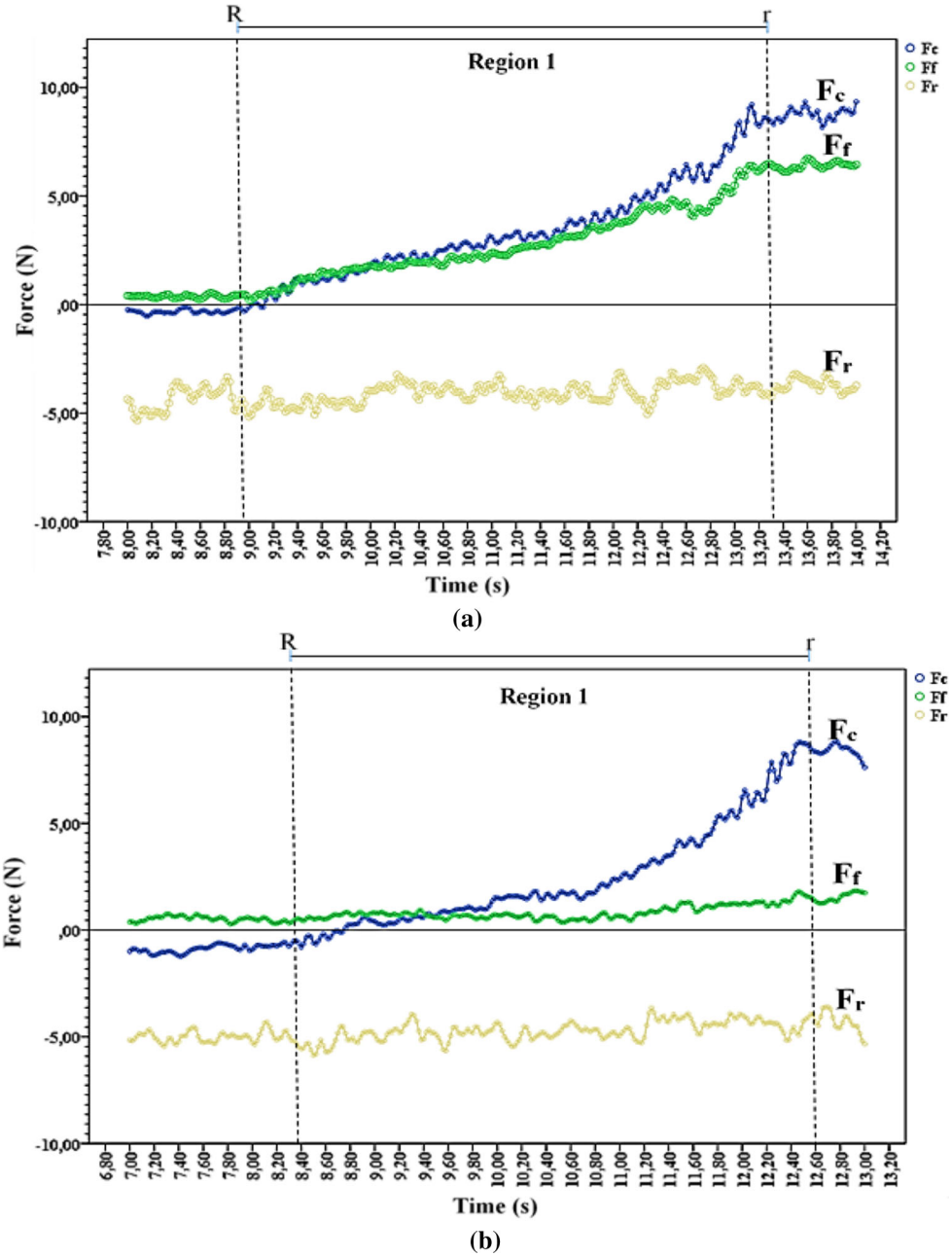

Fig. 11 The cutting forces acted on the cutting tool at 0° side cutting edge angle for 555 rpm machining operation (detailed view of the region 1 for **a** aluminum and **b** brass)

- According to the experimental measurements, it was understood that the force amplitudes were lower in Region 1 than in Region 2.
- The researchers who interest in impact loads in turning can tend to investigate not only intermittent workpieces but also prismatic parts.

Acknowledgements This study was financially supported by the Turkish Council of Higher Education under scholar grant: ÖYP-1919-020. The authors thank "Samsun Ilkadim Teknik ve Endüstri Meslek Lisesi" for using their facilities in our experiments. Special thanks to Nurettin ÜSTKOYUNCU, assistant professor at Electric Electronical Engineering, Department of Erciyes University, for his contributions of the strain gage based dynamometer design.

References

1. Yaldiz, S.; Unsacar, F.: A dynamometer design for measurement the cutting forces on turning. Measurement **39**(1), 80–89 (2006)
2. Korkut, I.: A dynamometer design and its construction for milling operation. Mater. Des. **24**(8), 631–637 (2003)
3. Gunay, M.; Aslan, E.; Korkut, I.; Seker, U.: Investigation of the effect of rake angle on main cutting force. Int. J. Mach. Tool Manuf. **44**(9), 953–959 (2004)
4. Gunay, M.; Korkut, I.; Aslan, E.; Seker, U.: Experimental investigation of the effect of cutting tool rake angle on main cutting force. J. Mater. Process. Technol. **166**(1), 44–49 (2005)
5. Gunay, M.; Seker, U.; Sur, G.: Design and construction of a dynamometer to evaluate the influence of cutting tool rake angle on cutting forces. Mater. Des. **27**(10), 1097–1101 (2006)

6. Radovanovic, M.; Dasic, P.; Jankovic, P.: Experimental determination of cutting force by longitudinal turning of C60E steel. Rom. Tech. Sci. Acad. **2**, 113–119 (2006)
7. Saglam, H.; Unsacar, F.; Yaldiz, S.: Investigation of the effect of rake angle and approaching angle on main cutting force and tool tip temperature. Int. J. Mach. Tool Manuf. **46**(2), 132–141 (2006)
8. Saglam, H.; Yaldiz, S.; Unsacar, F.: The effect of tool geometry and cutting speed on main cutting force and tool tip temperature. Mater. Des. **28**(1), 101–111 (2007)
9. Bajic, D.; Lela, B.; Cukor, G.: Examination and modelling of the influence of cutting parameters on the cutting force and the surface roughness in longitudinal turning. Stroj Vestn-J. Mech. E **54**(5), 322–333 (2008)
10. Thiele, J.D.; Melkote, S.N.: Effect of cutting edge geometry and workpiece hardness on surface generation in the finish hard turning of AISI 52100 steel. J. Mater. Process. Technol. **94**(2–3), 216–226 (1999)
11. Lin, W.S.; Lee, B.Y.; Wu, C.L.: Modeling the surface roughness and cutting force for turning. J. Mater. Process. Technol. **108**(3), 286–293 (2001)
12. Habalı, K.; Gökkaya, H.; Sert, H.: Experimental investigation of the effects of cutting tool coating materials on surface roughness in machining of AISI 1040 steel. J. Polytech. **9**(1), 35–38 (2006)
13. Nalbant, M.; Altin, A.; Gokkaya, H.: The effect of coating material and geometry of cutting tool and cutting speed on machinability properties of Inconel 718 super alloys. Mater Design **28**(5), 1719–1724 (2007)
14. Korkut, I.; Boy, M.: Experimental examination of main cutting force and surface roughness depending on cutting parameters. Stroj Vestn-J. Mech. E **54**(7–8), 531–538 (2008)
15. Asano, K.: Turning machinability of short alumina fiber reinforced aluminum alloy composite using carbide tool. Mater. Trans. **56**(7), 1120–1126 (2015)
16. Dinesh, S.; Senthilkumar, V.; Asokan, P.; Arulkirubakaran, D.: Effect of cryogenic cooling on machinability and surface quality of bio-degradable ZK60 Mg alloy. Mater. Des. **87**, 1030–1036 (2015)
17. Razavykia, A.; Farahany, S.; Yusof, N.M.: Evaluation of cutting force and surface roughness in the dry turning of Al–Mg_2i in-situ metal matrix composite inoculated with bismuth using DOE approach. Measurement **76**, 170–182 (2015)
18. Liu, X.W.; Cheng, K.; Webb, D.; Luo, X.C.: Prediction of cutting force distribution and its influence on dimensional accuracy in peripheral milling. Int. J. Mach. Tool Manuf. **42**(7), 791–800 (2002)
19. Topal, E.S.; Cogun, C.: A cutting force induced error elimination method for turning operations. J. Mater. Process. Technol. **170**(1–2), 192–203 (2005)
20. Cakir, M.C.; Isik, Y.: Detecting tool breakage in turning AISI 1050 steel using coated and uncoated cutting tools. J. Mater. Process. Technol. **159**(2), 191–198 (2005)
21. Denkena, B.; Lucas, A.; Bassett, E.: Effects of the cutting edge microgeometry on tool wear and its thermomechanical load. CIRP Ann. Manuf. Technol. **60**(1), 73–76 (2011)
22. Karpuschewski, B.; Schmidt, K.; Beno, J.; Mankova, I.; Frohmuller, R.; Prilukova, J.: An approach to the microscopic study of wear mechanisms during hard turning with coated ceramics. Wear **342**, 222–233 (2015)
23. Lin, H.S.; Wang, C.Y.; Yuan, Y.H.; Chen, Z.H.; Wang, Q.M.; Xiong, W.Q.: Tool wear in Ti–6Al–4V alloy turning under oils on water cooling comparing with cryogenic air mixed with minimal quantity lubrication. Int. J. Adv. Manuf. Technol. **81**(1–4), 87–101 (2015)
24. Milfelner, A.; Cus, F.; Balic, J.: An overview of data acquisition system for cutting force measuring and optimization in milling. J. Mater. Process. Technol. **164**, 1281–1288 (2005)
25. Kong, M.C.; Axinte, D.A.; Wilson, B.; Marinescu, I.; Allen, J.; Raffles, M.; Weston, S.: An innovative design of multi-task dynamometers for turning operations. Proc. Inst. Mech. Eng. B J. Eng. **226**(B6), 1118–1124 (2012)
26. Ayomoh, M.K.O.; Abou-EI-Hossein, K.A.; Olufayo, O.A.: Cutting force prediction for single point diamond tool-tip. In: 2013 6th Robotics and Mechatronics Conference (Robmech), pp. 123–128 (2013)
27. Teti, R.; Jemielniak, K.; O'Donnell, G.; Dornfeld, D.: Advanced monitoring of machining operations. CIRP Ann. Manuf. Technol. **59**(2), 717–739 (2010). https://doi.org/10.1016/j.cirp.2010.05.010
28. Yaldiz, S.; Unsacar, F.: Design, development and testing of a turning dynamometer for cutting force measurement. Mater. Des. **27**(10), 839–846 (2006). https://doi.org/10.1016/j.matdes.2005.04.001
29. Panzera, T.H.; Souza, P.R.; Rubio, J.C.C.; Abrao, A.M.; Mansur, T.R.: Development of a three-component dynamometer to measure turning force. Int. J. Adv. Manuf. Technol. **62**(9–12), 913–922 (2012). https://doi.org/10.1007/s00170-011-3866-5
30. Zhao, Y.; Zhao, Y.L.; Liang, S.B.; Zhou, G.W.: A high performance sensor for triaxial cutting force measurement in turning. Sensors Basel **15**(4), 7969–7984 (2015). https://doi.org/10.3390/s150407969
31. Hanif, M.I.; Aamir, M.; Muhammad, R.; Ahmed, N.; Maqsood, S.: Design and development of low cost compact force dynamometer for cutting forces measurements and process parameters optimization in turning applications. Int. J. Innov. Sci. **3**(9), 306–3016 (2015)
32. Öztürk, E.; Yıldızlı, K.: A new static calibration methodology for strain gage integrated dynamometers. Int. J. Adv. Manuf. Technol. **91**(5), 1823–1838 (2017)
33. Bouzakis, K.D.; Michailidis, N.; Skordaris, G.; Bouzakis, E.; Biermann, D.; M'Saoubi, R.: Cutting with coated tools: coating technologies, characterization methods and performance optimization. CIRP Ann. Manuf. Technol. **61**(2), 703–723 (2012)
34. Kurt, A.; Yalcin, B.; Yilmaz, N.: The cutting tool stresses in finish turning of hardened steel with mixed ceramic tool. Int. J. Adv. Manuf. Technol. **80**(1–4), 315–325 (2015)
35. Nalbant, M.; Altin, A.; Gokkaya, H.: The effect of cutting speed and cutting tool geometry on machinability properties of nickel-base Inconel 718 super alloys. Mater. Des. **28**(4), 1334–1338 (2007)
36. Dorlin, T.; Fromentin, G.; Costes, J.P.: Analysis and modelling of the contact radius effect on the cutting forces in cylindrical and face turning of Ti6Al4V titanium alloy. Proc. CIRP **31**, 185–190 (2015). https://doi.org/10.1016/j.procir.2015.03.017
37. Su, Y.; Li, Z.; Li, L.; Wang, J.; Gao, H.; Wang, G.: Cutting performance of micro-textured polycrystalline diamond tool in dry cutting. J. Manuf. Process. **27**, 1–7 (2017). https://doi.org/10.1016/j.jmapro.2017.03.013
38. Cui, X.B.; Zhao, J.; Zhou, Y.H.; Pei, Z.Q.: Cutting forces and tool wear in intermittent turning processes with Al_2O_3-based ceramic tools. Key Eng. Mater. **499**, 205–210 (2012). https://doi.org/10.4028/www.scientific.net/KEM.499.205
39. Gutnichenko, O.; Agic, A.; Stahl, J.E.: Modeling of force build-up process and optimization of tool geometry when intermittent turning. In: 16th CIRP Conference on Modelling of Machining Operations (16th Cirp Cmmo), vol. 58, pp. 393–398 (2017). https://doi.org/10.1016/j.procir.2017.03.241
40. Pressure gauges. https://dir.indiamart.com/impcat/electrical-pressure-gauges.html. Accessed 18 Apr 2017
41. Günay, M.: Talaş Kaldırma İşlemlerinde Kesici Takım Talaş Açısının Kesme Kuvvetlerine Etkisinin Deneysel Olarak İncelemesi. Gazi University (2003)
42. Öztürk, E.: Prizmatik Parçaların İşlenmesinde Kesme Kuvvetlerinin Analizi. Ondokuz Mayıs University (2015)